AN X-RAY DIP IN THE X-RAY TRANSIENT 4U 1630−47

J. A. TOMSICK, I. LAPSHOV, AND P. KAARET

Department of Physics and Columbia Astrophysics Laboratory, Columbia University, 538 West 120th Street, New York, NY 10027;
jtomsick@phys.columbia.edu

ABSTRACT

An X-ray dip was observed during a 1996 *Rossi X-Ray Timing Explorer* observation of the recurrent X-ray transient 4U 1630−47. During the dip, the 2–60 keV X-ray flux drops by a factor of about 3, and, at the lowest point of the dip, the X-ray spectrum is considerably softer than at nondip times. We find that the 4U 1630−47 dip is best explained by absorption of the inner part of an accretion disk, while the outer part of the disk is unaffected. The spectral evolution during the dip is adequately described by the variation of a single parameter, the column density obscuring the inner disk.

Subject headings: accretion, accretion disks — black hole physics — stars: individual (4U 1630−47) — X-rays: stars

1. INTRODUCTION

Dips have been observed in the X-ray light curves of about 20 X-ray binaries. The characteristics of the dips vary from source to source, requiring a number of different explanations for the dips. In many cases, dips are explained by absorption of the X-ray source by material passing in front of the source (White, Nagase, & Parmar 1995). In some sources, dips may be due to accretion disk instabilities, which cause the ejection of the inner part of the disk (Belloni et al. 1997; Greiner, Morgan, & Remillard 1996).

Here we present an analysis of an X-ray dip observed in the 1996 outburst of 4U 1630−47. The transient X-ray source 4U 1630−47 has been identified as a black hole candidate, on the basis of the shape of its X-ray spectrum and the lack of type I X-ray bursts (Parmar, Stella, & White 1986). 4U 1630−47 is unusual among X-ray transients because its outburst recurrence time is relatively short and regular, staying between 600 and 700 days (Kuulkers et al. 1997b). Although optical observations of 4U 1630−47 have been made (Parmar et al. 1986), an optical companion has not been identified. It has been suggested that 4U 1630−47 may be a superluminal radio jet source similar to GRS 1915+105 and GRO J1655−40, based on its timing properties (Kuulkers, van der Klis, & Parmar 1997c). For this reason, it is interesting to compare the properties of the 4U 1630−47 dip to the dips in GRS 1915+105.

In this paper, § 2 includes a description of the 4U 1630−47 observations and data analysis. In § 3 the results of the analysis are presented, and two possible causes for the dip are considered. We find that the dip can be explained by absorption of part of the X-ray source. In § 4 we discuss the implications of the dip.

2. OBSERVATIONS AND ANALYSIS

The X-ray transient 4U 1630−47 was observed with the *Rossi X-Ray Timing Explorer* (*RXTE*) (Bradt, Rothschild, & Swank 1993) several times during an outburst that began in 1996 March and lasted for 115 days (Levine et al. 1996a). In addition to the continual coverage provided by the All-Sky Monitor (ASM) (Levine et al. 1996b), 15 pointed observations were made between UTC 1996 May 3, 20:49:34 and UTC 1996 June 4, 20:22:13 with *RXTE*.

The typical on-source time for a pointed observation is 3000 s. Proportional Counter Array (PCA) (Jahoda et al. 1996) 2–60 keV light curves were produced with 0.5 s time bins for all of the pointed observations of 4U 1630−47 in order to look for X-ray dips. Based on a visual inspection of these light curves, we conclude that the only X-ray dips which occurred during the pointed observations were those observed during the May 3 observation. In this paper, we focus on data from the PCA for the first 1200 s of the pointed observation beginning UTC 1996 May 3, 20:49:34.

The PCA light curves for the 1200 s following UTC 1996 May 3, 20:49:34 (MJD 50,206.8679188), shown in Figure 1, were produced using B_2ms_16A_0_35_Q mode data, which provide 16 energy bins from 2–13.1 keV and 0.001953125 s time resolution. The light curves include the combined count rates for five PCUs and are background subtracted. During the May 3 observation, the nondip source flux is about 240 mcrab (2–60 keV), corresponding to a flux of 7.0×10^{-9} ergs cm^{-2} s^{-1}.

Energy spectra have been produced using Standard 2 PCA data and the Version 2.02 response matrix. This response matrix gives much better fits to the Crab for PCUs 0, 2, 3, and 4 than for PCU 1. Also, based on spectral fits to the Crab, the response matrix is much better for the top xenon layer than for the other two xenon layers. Thus, only data from the top xenon layers of PCUs 0, 2, 3, and 4 have been used in making energy spectra. A systematic error of 1% is assumed to account for uncertainties in the response matrix (Jahoda et al. 1997). Background subtraction has been performed including estimates for both the particle and the X-ray background (Stark et al. 1997). Spectral fits have been calculated using the XSPEC software (Shafer et al. 1991).

3. RESULTS

Figures 1*a*, 1*b*, and 1*c* show light curves binned in 1 s intervals for three energy bands: 2–3.8 keV (soft band), 3.8–5.7 keV (middle band), and 5.7–13.1 keV (hard band). We identify four dipping events in the X-ray light curve, which are labeled in Figure 1*a*: a short dip with a duration of ∼6 s labeled "1," a longer dip lasting ∼140 s labeled "2," and two more short dips labeled "3" and "4." During dip 2, the 2–60 keV X-ray flux decreases by a factor of 3.
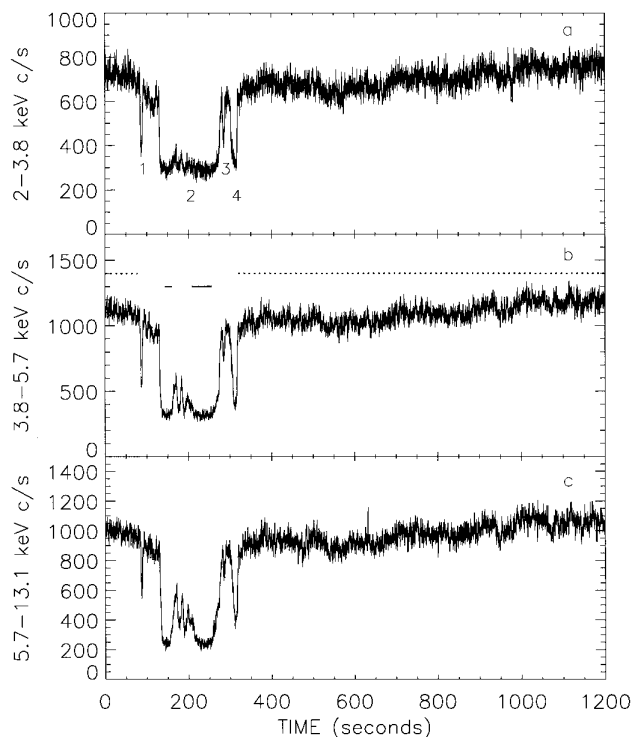
FIG. 1.—*RXTE* PCA light curves of 4U 1630−47 in (*a*) 2–3.8 keV, (*b*) 3.8–5.7 keV, and (*c*) 5.7–13.1 keV energy bands with 1 s time resolution. The starting time is UTC 1996 May 3, 20:49:34. In (*b*) the solid horizontal lines mark the dip times, and the dotted horizontal lines mark the nondip times used for spectral analysis.

Here we consider two possible causes for the dips: absorption or ejection of the inner part of the disk via an accretion disk instability.

Exponential fits to the light curves during ingress and egress of dip 2 have been calculated in order to compare the *e*-folding times for the three energy bands. For the ingress fits, 23 s of data after the start of dip 2 were used; for the egress fits, 57 s of data preceding the end of dip 2 were used. Table 1 shows the *e*-folding times and the values of χ_v^2 for the six fits. For both ingress and egress, there is a significant increase in *e*-folding time with increasing energy, suggesting that dip 2 is due to absorption by an object which has a lower column density at its edges than in its interior. This result does not appear to be consistent with dip 2 being caused by ejection of the inner disk, since it is difficult to see how the soft X-ray–emitting region could be ejected before

the hard X-ray–emitting region. Also, it is not clear why the hardest part of the X-ray source would recover first at the end of the dip. We also find that the egress *e*-folding times are substantially longer than the ingress *e*-folding times. If absorption is the cause of the dip, this result may indicate an asymmetry in the density or the shape of the absorber.

Figure 2 shows the relationship between spectral hardness and count rate. The hardness ratio is constant above about 1500 s^{-1}. However, as the count rate decreases from its nondip level, spectral changes become apparent. For intermediate count rates (1000 s^{-1} to 1500 s^{-1}) the spectrum is significantly harder than in its nondip state, and for count rates below 1000 s^{-1} the spectrum softens. The hardness increase at intermediate count rates is consistent with absorption but is inconsistent with ejection of the inner part of the accretion disk. The softening of the spectrum at count rates below 1000 s^{-1} can be explained by ejection of the inner part of the disk, but cannot be explained by a cold absorber covering the entire X-ray source. However, the softening is consistent with the presence of an extended soft X-ray source and provides motivation for a two-component model where one component is absorbed during the dip and a second, softer, extended component is not absorbed during the dip.

For spectral analysis, dip and nondip data have been selected from the May 3 observation based on the source intensity during each of the 16 s integrations provided by Standard 2 data. The dip spectrum consists of a 64 s integration, and 960 s of data are used for the nondip spectrum. For the nondip spectrum, single-component models do not provide acceptable fits: a power-law fit gives $\chi_v^2 = 14$ for 41 degrees of freedom (dof), a fit using a thermal bremsstrahlung model gives $\chi_v^2 = 14$ for 41 dof, a blackbody disk model gives $\chi_v^2 = 38$ for 41 dof, and a cutoff power law gives $\chi_v^2 = 4.3$ for 40 dof. An acceptable fit to the energy spectrum is achieved using a model combining a disk-blackbody component (Makishima et al. 1986) with a power-law component ($\chi_v^2 = 0.68$ for 39 dof). This is consistent with fits to spectra from previous observations of 4U 1630−47 (Parmar et al. 1997).

TABLE 1

INGRESS AND EGRESS *e*-FOLDING TIMES

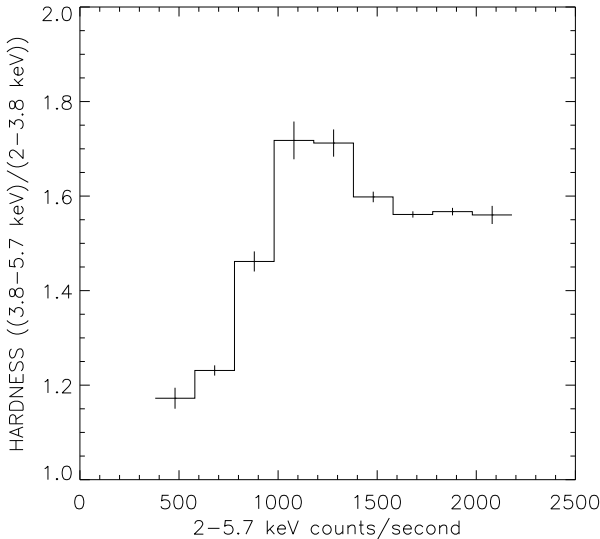| Energy Band (keV)	*e*-Folding Time (s)	χ_v^2 (dof)
Ingress		
2–3.8	1.56 ± 0.09	1.013 (180)
3.8–5.7	2.09 ± 0.08	1.161 (180)
5.7–13.1	2.78 ± 0.10	1.032 (180)
Egress		
2–3.8	4.48 ± 0.15	1.158 (453)
3.8–5.7	6.49 ± 0.15	1.075 (453)
5.7–13.1	10.24 ± 0.25	1.199 (453)

FIG. 2.—The (3.8–5.7 keV)/(2–3.8 keV) hardness ratio vs. count rate for the first 500 s of the light curves shown in Fig. 1.

Since the data suggest the presence of a soft component that is not absorbed during the dip, we consider a model where flux coming from the outer region of the disk is not affected during the dip and the inner region of the disk is absorbed during the dip. The radius dividing the unabsorbed and absorbed regions of the disk is one of the free parameters in the model. The sharp cutoff between the unabsorbed and absorbed regions is an approximation of the actual physical system. However, the data are not of sufficient quality to distinguish between this model and a more complex model. Since it is not known where the power-law component originates, the model allows for part of the power-law component to come from the unabsorbed region and part to come from the absorbed region, but it is assumed that the power-law index (α) is the same in both regions.

The disk model used here is the disk-blackbody model discussed in Makishima et al. (1986). Using this model, we are able to break the disk into two pieces and absorb the spectra from the two pieces differently. For each piece, the unabsorbed spectrum can be written as

$$f_{\mathrm{disk}}(x_1, x_2, N, T_{\mathrm{max}}; E) = C_0 N \int_{x_1}^{x_2} x B[T(x); E]dx \ , \quad (1)$$

where $B[T(x); E]$ is the blackbody flux per unit photon energy from a unit surface area of temperature $T(x)$, x is the radial distance from the compact object in units of the inner radius of the disk (r_{in}), and x_1 and x_2 are respectively the inner and outer radii for the piece of the disk in units of the inner radius of the disk. The expression used for $T(x)$ is given in equation (3.23) of Pringle (1981). C_0 is a constant equal to $2\pi(1\mathrm{km}/10\mathrm{kpc})^2$. Given x_1 and x_2, the spectrum is determined by the two parameters N and T_{max}. N, the normalization parameter, is given by $[(r_{\mathrm{in}}/1\mathrm{km})/(d/10\mathrm{kpc})]^2 \cos i$, where d is the distance to the source and i is the disk inclination. T_{max} is equal to the disk temperature at a radius $(49/36)r_{\mathrm{in}}$ (Pringle 1981). Combining the disk component with the power-law component and including absorption gives

$$f(x_1, x_2, N, T_{\mathrm{max}}, A, \alpha, N_{\mathrm{H}}; E)$$

$$= e^{-\sigma(E)N_{\mathrm{H}}}\left[f_{\mathrm{disk}}(x_1, x_2, N, T_{\mathrm{max}}; E) + A\left(\frac{E}{1 \ \mathrm{keV}}\right)^{-\alpha} \right] \quad (2)$$

for the spectrum from the region between x_1 and x_2. The cross section $[\sigma(E)]$ includes both photoelectric absorption (Morrison & McCammon 1983) and Compton scattering. Combining the emission from the absorbed and unabsorbed regions gives

$$S = e^{-\sigma(E)N_{\mathrm{H}}}f\left(1.0, \frac{r_d}{r_{\mathrm{in}}}, N, T_{\mathrm{max}}, A_{\mathrm{in}}, \alpha, N_{\mathrm{H}}^{(\mathrm{is})}; E \right)$$

$$+ f\left(\frac{r_d}{r_{\mathrm{in}}}, \frac{r_{\mathrm{out}}}{r_{\mathrm{in}}}, N, T_{\mathrm{max}}, A_{\mathrm{out}}, \alpha, N_{\mathrm{H}}^{(\mathrm{is})}; E \right), \quad (3)$$

where $N_{\mathrm{H}}^{(\mathrm{is})}$ is the column density for interstellar absorption, N_{H} is the column density for the extra absorbing material obscuring the inner disk, and r_d is the radius dividing the absorbed and unabsorbed regions. We assume that N_{H} is the same for photoelectric absorption and Compton scattering. The parameter $r_{\mathrm{out}}/r_{\mathrm{in}}$ is fixed so that the X-ray flux from disk radii beyond r_{out} is negligible. In all, there are
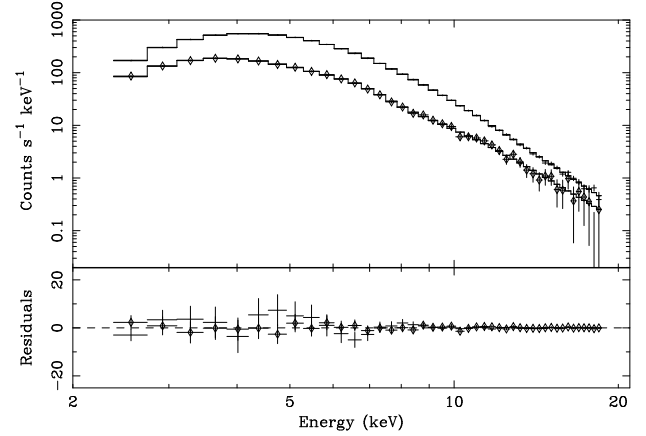

FIG. 3.—Dip and nondip *RXTE* PCA energy spectra. The dip spectrum and dip residuals are marked with diamonds. Dip and nondip times are defined in Fig. 1.

eight free parameters in the model. The unabsorbed emission from the disk is determined by N and T_{max}. The parameters A_{in}, A_{out}, and α specify the emission due to the power-law component. The other free parameters are $N_{\mathrm{H}}^{(\mathrm{is})}$, N_{H}, and r_d/r_{in}.

This model has been used to fit simultaneously the dip and nondip spectra. In calculating the fit, the only parameter that is allowed to be different for the two spectra is the column density (N_{H}) of the absorbing material. This model provides a good fit to the two spectra with $\chi_v^2 = 0.65$ for 79 dof. The fit parameters with their 68% confidence errors are given in Table 2, and the fitted spectra are shown in Figure 3. The extra material absorbing the inner region of the disk is found to have a column density of $N_{\mathrm{H}} = (86.8 \pm 4.4) \times 10^{22}$ cm^{-2} during the dip and $N_{\mathrm{H}} = (7.32 \pm 1.47) \times 10^{22}$ cm^{-2} during the nondip, and the interstellar absorption is $N_{\mathrm{H}}^{(\mathrm{is})} = (8.26 \pm 0.74) \times 10^{22}$ cm^{-2}. The nondip and dip spectra cannot be simultaneously fitted with a model where N_{H} is set to zero for the nondip and $N_{\mathrm{H}}^{(\mathrm{is})}$ is the same for the inner and outer regions of the disk.

Past observations of 4U 1630−47 show that it is reasonable to think that some portion of the absorption measured in the nondip spectrum is due to material close to the source, since the column density has shown a high degree of variability from observation to observation. Column den-

TABLE 2

FIT PARAMETERS FOR THE SIMULTANEOUS FIT TO THE DIP AND NONDIP SPECTRA

Parameter	Value	Dimensions
N	67.4 ± 6.7	Dimensionless
kT_{max}	1.145 ± 0.011	keV
A_{in}	78.1 ± 30.4	photons cm^{-2} s^{-1} keV^{-1}
A_{out}	2.7 ± 4.7	photons cm^{-2} s^{-1} keV^{-1}
α	4.20 ± 0.15	Dimensionless
$N_{\mathrm{H}}^{(\mathrm{is})}$	8.26 ± 0.74	10^{22} H atoms cm^{-2}
r_d/r_{in}	2.77 ± 0.10	Dimensionless
N_{H} (dip)	86.75 ± 4.39	10^{22} H atoms cm^{-2}
N_{H} (nondip)......	7.32 ± 1.47	10^{22} H atoms cm^{-2}

sities of $(6.4 \pm 0.2) \times 10^{22}$ cm^{-2}, $(9.51 \pm 0.11) \times 10^{22}$ cm^{-2}, and $(14.3 \pm 1.2) \times 10^{22}$ cm^{-2} were measured in three separate observations (Parmar, Angelini, & White 1995; Parmar et al. 1997). It would be reasonable to assume that the lowest of these measurements provides an upper limit on the interstellar absorption, which would make our value of $N_{\rm H}^{\rm (is)}$ only slightly higher than expected.

Above about 13 keV, the power-law component dominates the nondip and dip spectra, and the disk-blackbody component is negligible. Figure 3 shows that the dip flux is lower than the nondip flux at all energies, including the power-law–dominated region. Thus, if the dip is caused by absorption, then at least part of the power-law component must be absorbed. Comparing the values of $A_{\rm in}(78.1 \pm 30.4)$ and $A_{\rm out}(2.7 \pm 4.7)$ indicates that most of the power-law component comes from the absorbed region. Further evidence that most of the power-law component is absorbed is the fact that if $A_{\rm out}$ is fixed to zero, and the simultaneous fit is recalculated, the quality of the fit does not change ($\chi_v^2 = 0.65$ for 80 dof).

If the only parameter that changes with time is the column density of the absorber, a measured count rate in a particular energy band corresponds to a unique value of $N_{\rm H}$, and it is possible to see whether variations in the column density can produce the features observed in the light curves shown in Figure 1. Figure 4 shows the column density estimates derived from the count rates in the middle and hard bands during the dip. There is good agreement between the $N_{\rm H}$ values calculated from the two bands. The model predicts almost the same flux in the soft band for all values of $N_{\rm H}$ above about 40×10^{22} cm^{-2}; thus, for column densities above this level, the soft-band flux provides no information and is not shown in Figure 4. The absorption model predicts that the drop in the column density observed in the middle of dip 2 should produce a 20% increase in the soft-band flux. This is consistent with the observed 21.8%±2.7% flux increase. The model assumes

that the intrinsic (unabsorbed) intensity of 4U 1630−47 remains constant during the dips, and that the observed change in flux is due entirely to variations in the column density. Using the nondip light curve with 0.5 s time bins, we find that the source variability is below the 5% level over a time interval comparable to the duration of the dip (140 s), indicating that this assumption is reasonable.

A model where an accretion disk instability leads to ejection of the inner part of the accretion disk has been used to explain the X-ray dips observed in GRS 1915+105. Since this is a model which can produce spectrally soft dips, we have considered it as a possible mechanism for the 4U 1630−47 dip. Based on fits to GRS 1915+105 spectra, Belloni et al. (1997) found that the inner radius of the accretion disk is larger during dip times than during nondip times. We fit the 4U 1630−47 nondip and dip spectra simultaneously using a disk-blackbody plus power law model and requiring the absorption (column density and absorption-edge parameters) to be the same for the nondip and dip spectra. For the dip spectrum, the disk-blackbody normalization is consistent with zero (26 ± 36), and the power law is the only significant spectral component. This could be interpreted as meaning that the entire X-ray–emitting portion of the disk is ejected during the dip. However, large residuals are observed near 7 keV for the dip spectrum but not for the nondip spectrum. This suggests the presence of an iron K-absorption edge only in the dip spectrum, which supports absorption as the cause of the dip.

4. DISCUSSION

The spectrally soft X-ray dips observed in 4U 1630−47 are best explained by a model where part of the X-ray source is absorbed, while another part of the X-ray source is unaffected during the dips. The models used to explain absorption dips in other sources typically place the absorbing material in the accretion disk or in a wind from a high-mass companion. In the former case, the dips are probably produced by an accumulation of material where the stream of material from the companion impacts the disk. This results in dips being observed at certain orbital phases, and most of these sources are described as periodic dippers. In order for dips to be observed, the inclination angle must be relatively high ($i > 70°$) (White et al. 1995). Strong stellar winds often exist in binaries where the optical companion is an O- or B-type star. In 4U 1630−47, neither the inclination angle nor the spectral type of the companion is known, so there is no reason to assume either of these possibilities a priori. In this section, we discuss the properties of the dip in relation to these two possibilities.

Frank, King, & Lasota (1987, hereafter FKL) explain the dips using a model where the stream of material from the companion is thicker than the scale height of the accretion disk, so that a fraction of the stream flows above and below the disk. In this model, when the matter from the stream is irradiated by X-rays coming from close to the compact object, ionization instabilities cause the material to separate into a two-phase medium consisting of cold, relatively dense clouds, which are responsible for the dips, in a hot intercloud medium. Here we compare the cloud sizes and densities derived by FKL to estimates for those quantities for the absorber producing the dips in 4U 1630−47. To estimate the absorber velocity, we assume that the absorber is in a circular orbit about a 3 $M_\odot$ compact object, where the
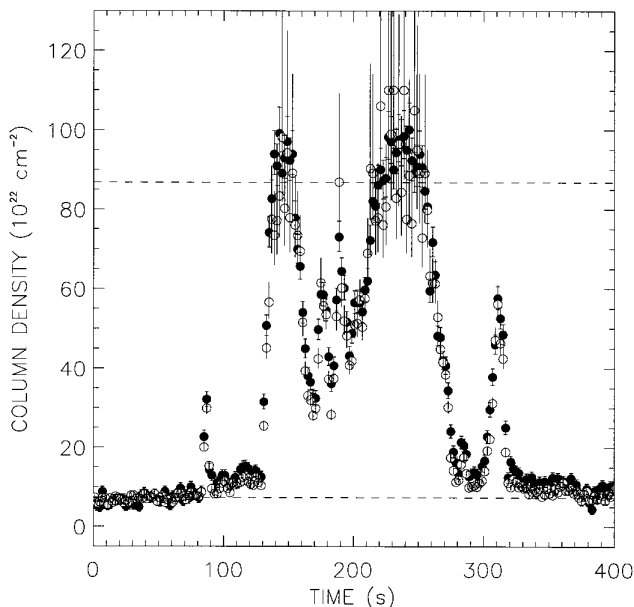

FIG. 4.—The filled circles are the column density estimates derived from the 5.7–13.1 keV count rates, and the open circles are the column density estimates from the 3.8–5.7 keV band. The dashed lines mark the dip and nondip values of $N_{\rm H}$.

mass estimate comes from assuming that the highest observed flux for 4U 1630−47 (Parmar et al. 1995) is the Eddington luminosity at 10 kpc. We use $r = 4.9 \times 10^{10} P_{1\,\text{day}}^{2/3}$ cm for the distance from the compact object to the absorber (FKL), where $P_{1\,\text{day}}$ is the binary orbital period in units of days. If we assume that a typical cloud caused dip 1, then the cloud diameter is $5.4 \times 10^{8} P_{1\,\text{day}}^{-1/3}$ cm. By using the dip 1 duration, we are assuming that dips 2 and 4 last longer and have higher peak column densities because they are caused by multiple clouds. Using standard values for the accretion rate, the fraction of matter in the incoming stream which reaches r, and the scale height of the disk given in FKL, the cloud sizes expected from the model of FKL are $6.4 \times 10^{8} P_{1\,\text{day}}^{11/9}$ cm for $M = 3\ M_{\odot}$, and the cloud size estimates agree if the orbital period is near 1 day.

We can estimate the density of the absorber that produced dip 1 if we assume that the linear size of the cloud along the line of sight is the same as the linear size in the direction perpendicular to the line of sight. For matter with cosmic abundances, the cloud density is found to be $1.6 \times 10^{-9} P_{1\,\text{day}}^{1/3}$ g cm^{-3}. Making the same assumptions as above, the density derived by FKL is $2.7 \times 10^{-9} P_{1\,\text{day}}^{-7/3}$ g cm^{-3}, and the density estimates agree if the orbital period of the system is near 1 day, which is consistent with the orbital period derived based on the sizes of the clumps. We conclude that the characteristics of the dip are consistent with being produced by material in the accretion disk and that the model of FKL may imply that the orbital period of 4U 1630−47 is about a day.

Finding that 4U 1630−47 dips periodically would be evidence that the dips are caused by material in the accretion disk. The other systems that exhibit periodic dips typically have duty cycles between 10% and 30%. Dips have never been observed before in 4U 1630−47, and the longest continuous observation was a 7 hr *EXOSAT* observation (Parmar et al. 1986). Thus, assuming that X-ray dipping is not a transient phenomenon in 4U 1630−47, the upper limit on the duty cycle is 1%. Recent observations of dips from the superluminal jet source GRO J1655−40 indicate that the dips in this source also have a very small duty cycle, 0.2% for 400 s dips every 2.6 days (Kuulkers et al. 1997a). Most of the systems that exhibit periodic dipping are neutron star X-ray binaries, while GRO J1655−40 is securely identified as a black hole system (Orosz & Bailyn 1997). The fact that the dip duty cycle in GRO J1655−40 is so different from the neutron star systems suggests the possibility that the difference is related to the nature of the compact object. The 4U 1630−47 duty cycle may be small because the source contains a black hole.

To fit the dip spectrum of 4U 1630−47 by absorbing the nondip spectrum, it is necessary to absorb the power-law component. This is in contrast to the X-ray burster 4U 1624−49 (Church & Balucińska-Church 1995), for which the nondip spectrum is fitted with a blackbody plus power

law model, and the dip spectrum can be fitted by absorbing the blackbody component but leaving the power-law component unaffected. These results probably indicate that the size of the region emitting the power law is larger for 4U 1624−49 than for 4U 1630−47 and may indicate that the size of the region emitting the power law is larger for neutron star systems than for systems containing black holes. It would be interesting to compare the spectral evolution of GRO J1655−40 during dips to that of 4U 1630−47 and 4U 1624−49.

We have also considered the possibility that the 4U 1630−47 dip is produced by a wind from a high-mass companion. For 4U 1630−47, the relatively sharp transitions between nondip and dip states, as observed in the light curve, and the corresponding variations in the column density indicate that the material producing the dips must be nonuniform in density and/or shape (i.e., clumpy); however, there is evidence for nonuniformity in stellar winds. Cyg X-1 is a high-mass X-ray binary (HMXB), where dips with sharp ingresses and egresses (~ 2 s) are observed and attributed to the wind from the high-mass companion (Kitamoto et al. 1984). In addition, Nagase et al. (1986) suggests that stellar winds are likely to be turbulent and that clumping may be caused or enhanced by the X-ray source. The typical column densities observed for dips in HMXBs are between 10×10^{22} and 50×10^{22} cm^{-2} (Haberl & White 1990; Kitamoto, Miyamoto, & Yamamoto 1989), which are only slightly less than the maximum column density measured for 4U 1630−47. Based on the properties of the dips observed in HMXBs, we cannot eliminate the possibility that the 4U 1630−47 dip was caused by material in the wind of a high-mass companion.

Distinguishing between the possible causes of the dip in 4U 1630−47 may lead to understanding its outburst recurrence time (t_r). It has been suggested that t_r may be the orbital period of the system and that outbursts occur near periastron (Parmar et al. 1995). Finding that material in a stellar wind was responsible for the dip would indicate the presence of a high-mass companion and make it likely that t_r is the orbital period. Alternatively, confirmation of an orbital period near 1 day suggests similarities between 4U 1630−47 and Her X-1, which has a 1.7 day orbital period and a 35 day on/off cycle. In this picture, t_r is analogous to the 35 day period in Her X-1, which is explained by accretion disk precession (Crosa & Boynton 1980). Kuulkers et al. (1997b) find evidence for a change in t_r from 600 to 690 days for the last three 4U 1630−47 outbursts, which suggests that t_r is not the orbital period. However, the behavior of the X-ray transient GS 0834−430 indicates that the possibility that t_r is related to the orbital period should not be completely ruled out (Wilson et al. 1997).

REFERENCES

Belloni, T., Mendez, M., King, A. R., van der Klis, M., & van Paradijs, J. 1997, ApJ, 479, L145
Bradt, H. V., Rothschild, R. E., & Swank, J. H. 1993, A&A, 97, 355
Church, M. J., & Balucińska-Church, M. 1995, A&A, 300, 441
Crosa, L., & Boynton, P. E. 1980, ApJ, 235, 999
Frank, J., King, A. R., & Lasota, J.-P. 1987, A&A, 178, 137 (FKL)
Greiner, J., Morgan, E. H., & Remillard, R. A. 1996, ApJ, 473, L107
Haberl, F., & White, N. E. 1990, ApJ, 361, 225
Jahoda, K., Swank, J. H., Giles, A. B., Stark, M. J., Strohmayer, T., Zhang, W., & Morgan, E. H. 1996, Proc. SPIE, 2808, 59

Jahoda, K., et al. 1997, XTE-PCA, http://lheawww.gsfc.nasa.gov/docs/xray/xte/pca
Kitamoto, S., Miyamoto, S., Tanaka, Y., Ohashi, T., Kondo, Y., Tawara, Y., & Nakagawa, M. 1984, PASJ, 36, 731
Kitamoto, S., Miyamoto, S., & Yamamoto, T. 1989, PASJ, 41, 81
Kuulkers, E., Belloni, T., Mendez, M., van der Klis, M., Wijnands, R., & van Paradijs, J. 1997a, IAU Circ. 6637
Kuulkers, E., Parmar, A. N., Kitamoto, S., Cominsky, L. R., & Sood, R. K. 1997b, MNRAS, 291, 81
Kuulkers, E., van der Klis, M., & Parmar, A. N. 1997c, ApJ, 474, L47

Levine, A. M., et al. 1996a, IAU Circ. 6390
Levine, A. M., Bradt, H., Cui, W., Jernigan, J. G., Morgan, E. H., Remillard, R., Shirey, R. E., & Smith, D. A. 1996b, ApJ, 469, L33
Makishima, K., et al. 1986, ApJ, 308, 635
Morrison, R., & McCammon, D. 1983, ApJ, 270, 119
Nagase, F., Satio, H., Sato, N., Masai, K., & Inoue, H. 1986, PASJ, 38, 547
Orosz, J. A., & Bailyn, C. 1997, ApJ, 477, 876
Parmar, A. N., Angelini, L., & White, N. E. 1995, ApJ, 452, L129
Parmar, A. N., Stella, L., & White, N. E. 1986, ApJ, 304, 664
Parmar, A. N., Williams, O. R., Kuulkers, E., Angelini, L., & White, N. E. 1997, A&A, 319, 855

Pringle, J. E. 1981, ARA&A, 19, 137
Shafer, R. A., Haberl, F., Arnaud, K. A., & Tennant, A. F. 1991, XSPEC User's Guide (ESA TM-09; Paris: ESA)
Stark, M., et al. 1997, PCABACKEST, http://lheawww.gsfc.nasa.gov/docs/xray/xte/pca
White, N. E., Nagase, F., & Parmar, A. N. 1995, in X-Ray Binaries, ed. W. H. G. Lewin, J. van Paradijs, & E. P. J. van den Heuvel (Cambridge: Cambridge Univ. Press), 1
Wilson, C. A., Finger, M. H., Harmon, B. A., Scott, D. M., Wilson, R. B., Bildsten, L., Chakrabarty, D., & Prince, T. A. 1997, ApJ, 479, 388